Optimal Sensor Selection for Jammer Identification

Andreas Jansson and Andreas Jakobsson
Dept. of Mathematical Sciences, Lund University, Sweden

***Abstract*—Deception jamming is a powerful technique used to disrupt various radar systems. In this work, we propose a novel sensor selection scheme for FDA-MIMO radar systems designed to maximize the likelihood of accurate jammer identification. The approach exploits the inherent delay between a jammer measuring incoming waveforms and its response. This delay induces a slight shift in the perceived distance across different receivers, known as the deception range, enabling differentiation between jammers and true targets. The proposed sensor selection scheme is formulated to minimize the achievable variance of the deception range, enhancing identification accuracy.**

***Index Terms*—FDA-MIMO radar, Jammer detection, Optimal sensor selection, Deception range**

I. Introduction

Deception jamming is a simple but efficient technique for disrupting many forms of radar systems [1], [2]. This form of jammers can intercept, modulate, and retransmit incoming radar signals to create false targets that closely resemble real ones [3]–[6]. This capability enables the jammer to actively manipulate the perceived number, location, and velocity of reflections detected by the interrogating radar system. In order to alleviate such interference, it is critical that the radar system identifies which reflections corresponds to real targets and which are the results of a deceptive jammer.

Given the importance of the topic, this has resulted in several studies with this focus. Such works include the interference suppression method using data-independent beamforming that was proposed in [7], employing a minimum redundancy array design for transmitting. As an alternative, an electronic counter-countermeasures technique against velocity deception jamming was proposed in [8], where an approach to estimate the parameters of the false targets was also presented. A three-dimensional joint domain localized space-time adaptive processing (STAP) method, together with deception jamming pre-whitening was proposed in [9] to deal with performance degradation in the presence of dense false target jamming. In [10], an adaptive suppression technique was introduced that exploited random permutations of the frequency increments of a frequency diverse array (FDA).

Several of these studies exploit FDA multiple-input multiple-output (MIMO) radar systems, an area that has recently attracted notable interest, not least due to such systems' capability to suppress mainlobe interference [11], [12], but also due to the ability to jointly estimate both range and angle to a target [13]. A key aspect of FDA is that more degrees of freedom in the range dimension are available to focus the beam in the range-angle plane. This comes at the cost of a more involved processing of the signals due to potentially aliased multi-carrier signals.

Another area that has attracted increasing interest is the optimal selection of sensors. For many applications, such as localization and target identification, the choice of sensor placements is critical [14]–[18]. Clearly, some sensor placements are more suitable than others, and several works have examined how the sensor placement may be done optimally. Most of the noted approaches exploit some form of minimization of the corresponding Cramér-Rao lower bound (CRLB) in order to select the placement that yields the theoretically lowest parameter variance. Most commonly, these approaches employ *A-optimality*, minimizing the sum of the eigenvalues of the CRB. Given the difference in scale and importance between the different radar parameters, it is often beneficial to also form the optimization so that the relevant parameters may be appropriately emphasized [16], [19].

In this paper, we combine these two areas of study, examining the optimal sensor selection for determining whether the impinging reflections result from true targets or from deceptive jammers. To do so, we combine the (A-optimal) sensor selection scheme developed in [16], [19], allowing for parameter selection with a signal structure emphasizing the deception range resulting from the inevitable processing delay of the jammers. By being able to accurately determine the deception range, an estimator will be able to improve the differentiation between targets and jammers. As the ability to determine the deception range necessitates an accurate estimation of the other radar parameters, the determined sensor selection scheme will also yield a suitable sensor selection for these parameter, as is also demonstrated, even though this is not emphasizes in the resulting optimization.

The remainder of the paper is organized as follows: in the next section, we present the signal model taking into account the deception range of the jammers. Then, in Section III, we introduce the optimal sensor selection scheme emphasizing the estimation performance of the deception range. Section IV contains numerical simulations illustrating the achieved performance gain as compared to selecting the sensors randomly 10.000 times and picking the best selection. Finally, we conclude on the work in Section V.

II. Signal model

Consider M transmitters and N receivers, measuring signals resulting from Q targets, with the mth transmitter and the nth receiver being located at

$$\mathbf{m}_m^{\mathcal{T}} = \begin{bmatrix} x_m^{\mathcal{T}} & y_m^{\mathcal{T}} \end{bmatrix}^T, \quad m = 1, \cdots, M \tag{1}$$

$$\mathbf{m}_n^{\mathcal{R}} = \begin{bmatrix} x_n^{\mathcal{R}} & y_n^{\mathcal{R}} \end{bmatrix}^T, \quad n = 1, \cdots, N \tag{2}$$

respectively, with $[\cdot]^T$ denoting the transpose. The kth radar pulse from the mth transmitter is formed as

$$x_{mk}(t) = \sqrt{\frac{E}{M}} s_m\left(t-(k-1)T\right) W_k\left(t\right) \tag{3}$$

where $k = 1, \cdots, K$, with K being the number of pulses, E denotes the total transmitting energy, $s_m(t)$ is the baseband signal with pulse repetition interval (PRI) T and bandwidth B_s, whereas $W_k\left(t\right)$ defines a rectangular window, i.e.,

$$W_k\left(t\right) = \begin{cases} 1, & (k-1)T < t \leq kT \\ 0, & \text{otherwise} \end{cases} \tag{4}$$

In order to be able to separate the transmitted pulses at the receivers, the transmitted signals are formed to be (at least approximatively) orthogonal, i.e.,

$$\int_{T_d} s_m\left(t\right) s^*_{m'}\left(t+t'\right) dt = \begin{cases} 1, & m = m' \\ 0, & \text{otherwise} \end{cases} = \delta_{mm'} \tag{5}$$

where t' is assumed to be small, T_d is the duration of the waveform with $T_d \leq T$, and δ_{mn} is the Kronecker delta. Let τ^q_{mnk} denote the propagation time delay for the kth pulse of the mth transmitter to reach the qth target and be backscattered to the nth receiver, with

$$\tau^q_{mnk} = \frac{\left\|\mathbf{m}^{\mathcal{T}}_m - \boldsymbol{\rho}^q_k\right\|_2 + \left\|\mathbf{m}^{\mathcal{R}}_n - \boldsymbol{\rho}^q_k\right\|_2}{c} \tag{6}$$

where $\boldsymbol{\rho}^q_k = [x^q_k \quad y^q_k]^T$ is the location of the qth target at pulse number k.

Allowing for the motion of the reflectors, the received signal will experience a Doppler shift, ν^q_{mnk}, formed as [4]

$$\nu^q_{mnk} = -\frac{f^m_c}{c}\left[\Delta^x_{mnk} + \Delta^y_{mnk} + \varepsilon^q_k\right] \tag{7}$$

$$\Delta^x_{mnk} = \cos\Big(\varphi^q_{mk} + \phi^q_{nk}\Big)\dot{x}^q_k \tag{8}$$

$$\Delta^y_{mnk} = \sin\Big(\varphi^q_{mk} + \phi^q_{nk}\Big)\dot{y}^q_k \tag{9}$$

where f^m_c denotes the carrier frequency of the mth transmitter and φ^q_{mk} and ϕ^q_{nk} are the target bearing angles at the transmitter and receiver with respect to x axis, respectively, i.e.,

$$\varphi^q_{mk} = \text{atan2}\Big\{\left(y^q_k - y^{\mathcal{T}}_m\right), \left(x^q_k - x^{\mathcal{T}}_m\right)\Big\} \tag{10}$$

$$\phi^q_{nk} = \text{atan2}\Big\{\left(y^q_k - y^{\mathcal{R}}_n\right), \left(x^q_k - x^{\mathcal{R}}_n\right)\Big\}, \tag{11}$$

with atan2$(\cdot)$ denoting the 2-argument arctangent function. Then, the signal received by nth receive sensor at the kth pulse for the qth target may be expressed as

$$\begin{aligned} \tilde{y}^q_{nk}\left(t\right) &= \sum_{m'=1}^{M} \alpha^q_{m'n} x_{m'k}(t - \tilde{\tau}^q_{m'nk}) e^{j2\pi\nu^q_{m'nk}t} \\ &= \sum_{m'=1}^{M} \tilde{\alpha}^q_{m'n} s_{m'}(t - \tilde{\tau}^q_{m'nk} - k_T)\times \\ &\qquad e^{j2\pi\nu^q_{m'nk}t} W_k(t - \tilde{\tau}^q_{m'nk}) \end{aligned} \tag{12}$$

where

$$\tilde{\alpha}^q_{m'n} = \sqrt{E/M}\alpha^q_{m'n}, \tag{13}$$

$$\tilde{\tau}^q_{m'nk} = \tau^q_{m'nk} + r^q_k/c, \tag{14}$$

$$k_T = (k-1)T, \tag{15}$$

with $\alpha^q_{m'n}$ denoting the (unknown) complex-valued reflectivity coefficient accounting for the radar cross section (RCS) of the target and r^q_k denoting the deception range; for a true target this will thus be zero, whereas for a jammer it will be non-zero due to the inevitable internal processing delay of the jammer. Forming the transmitted signal as

$$s_m(t) = e^{j2\pi(f^m_c t + (B_s/T_p)t^2)} = e^{j2\pi f^m_c t} u(t), \tag{16}$$

where $u(t) = e^{j2\pi(B_s/T_p)t^2}$ denotes the baseband emitted signal, the demodulated signal may be expressed as

$$\begin{aligned} \tilde{z}^q_{mnk}(t) &= \tilde{y}^q_{nk}(t) e^{-j2\pi f^m_c t} \\ &= \sum_{m'=1}^{M} \tilde{\alpha}^q_{m'n} s_{m'}(t - \tilde{\tau}^q_{m'nk} - k_T)\times \\ &\qquad e^{j2\pi(\nu^q_{m'nk} - f^m_c)t} W_k(t - \tilde{\tau}^q_{m'nk}) \end{aligned} \tag{17}$$

Matched filtering with the baseband signal then yields

$$\begin{aligned} \breve{z}^q_{mnk}(\tau) &= \int_{T_p} \tilde{z}^q_{mnk}(t+\tau) u^*(t) dt \\ &\approx \tilde{\alpha}^q_{mn} e^{j2\pi(\nu^q_{mnk} - f^m_c)\tau} \Lambda_m(\tau, \tilde{\tau} + k_T) \end{aligned} \tag{18}$$

where

$$\begin{aligned} \Lambda_m(\tau, \tau') &= \int_{T_p} s_m(t + \tau - \tau') s^*_m(t) dt \\ &= \frac{1}{j4\pi\mu(\tau - \tau')}\left[e^{j4\pi\mu(\tau-\tau')t}\right]^{t=b}_{t=a} \\ &= \frac{e^{j4\pi\mu(\tau-\tau')b} - e^{j4\pi\mu(\tau-\tau')a}}{j4\pi\mu(\tau - \tau')} \end{aligned} \tag{19}$$

with $\mu = B_s/T_p$, $a = \max(\tau, \tau')$, and $b = \min(\tau, \tau') + T_p$. Thus, at the pth range bin, $\tau = pt_s$, with $t_s = 1/f_s$, where f_s denotes the sampling frequency, the preprocessed signal may be expressed as

$$z^p_{mnk} = \sum_q \breve{z}^{qp}_{mnk} + w^p_{mnk} \tag{20}$$

where $\breve{z}^{qp}_{mnk} = \breve{z}^q_{mnk}(pt_s)$ and w^p_{mnk} denotes an additive noise that is here assumed to be well modelled as a zero-mean circularly symmetric white Gaussian noise, i.e., $w^p_{mnk} \sim \mathcal{CN}(0, \sigma^2_w)$.

III. Optimal Sensor Selection

Assuming that there are M fixed transmitters (TX) and that N receivers (RX) are selected from the sensor set $\mathcal{M} = \{1, \ldots, \Upsilon\}$ of potential candidate locations, the unknown parameters detailing the system are

$$\boldsymbol{\xi} = [\boldsymbol{\xi}^T_1 \quad \ldots \quad \boldsymbol{\xi}^T_K \quad \sigma^2_w]^T \tag{21}$$

where $\boldsymbol{\xi}_k = [(\boldsymbol{\Theta}_k^1)^T \quad \dots \quad (\boldsymbol{\Theta}_k^Q)^T]^T$ and

$$\boldsymbol{\Theta}_k^q = [x_k^q \quad y_k^q \quad \dot{x}_k^q \quad \dot{y}_k^q \quad r_k^q \quad \varepsilon_k^q \quad \alpha_k^q]^T. \tag{22}$$

In order to select optimal RX sensor placements for determining if a reflector is formed by a true target or a jammer, we consider a setup containing Υ potential sensor locations, as illustrated in Figure 1. The sought target identification may then be determined by estimating the perceived deception range of each reflector, as the true targets should have a negligible deception range whereas any jammer will necessarily have a non-zero deception range. The theoretical minimum achievable variance of the involved parameter estimates may be expressed as a function of the Fisher information matrices (FIMs) corresponding to each potential sensor placement. For an RX candidate position n, the corresponding FIM may be expressed as

$$\begin{aligned}\mathbf{FIM}_n(\boldsymbol{\xi}) &= -\mathbb{E}\left[\boldsymbol{\nabla}_{\boldsymbol{\xi}}\boldsymbol{\nabla}_{\boldsymbol{\xi}}^T \log p(\mathbf{z}_n)\right] \\ &= \frac{2}{\sigma_w^2}\sum_{m,k,p}\left(\Re\left\{\boldsymbol{\nabla}_{\boldsymbol{\xi}} z_{mnk}^p \boldsymbol{\nabla}_{\boldsymbol{\xi}}^H (z_{mnk}^p)\right\}\right) \\ &= \sum_{m,k,p}\mathbf{FIM}_{mnk}^p(\boldsymbol{\xi}) = \mathbf{F}_n(\boldsymbol{\xi})\end{aligned} \tag{23}$$

where $\mathbf{z}_n$ is the vector of z_{mnk}^p over p, k, and m (in that order), $\boldsymbol{\nabla}_{\boldsymbol{\xi}}$ denotes the gradient with respect to $\boldsymbol{\xi}$, $\Re\{\cdot\}$ the real part, and $p(\mathbf{z}_n)$ is the probability density function (PDF) of the data. Reminiscent of the optimal sampling problems formulated in [16], [19], the optimal sensor selection may then be formed using A-optimality, i.e., by minimizing the trace of the resulting error covariance matrix, i.e.,

$$\begin{aligned}\min_{\mathbf{w}} \quad & \text{trace}\left(\left(\sum_{n=1}^{\Upsilon} w_n \mathbf{F}_n(\boldsymbol{\xi})\right)^{-1}\right) \\ \text{subject to} \quad & \mathbf{1}^T\mathbf{w} \leq N, \\ & w_n \in \{0,1\}, n = 1,2,\dots,\Upsilon = |\mathcal{M}|\end{aligned} \tag{24}$$

where $\mathbf{w}$ is the Υ-dimensional weight vector indicating if a candidate sensor placement in the set of potential candidate placements, $\mathcal{M}$, is used or not. The resulting problem is non-convex due to the binary nature of the selection variables. To form a computationally tractable approximation, one may instead use the convex relaxation

$$\begin{aligned}\min_{\mathbf{w}} \quad & \text{trace}\left(\left(\sum_{n=1}^{\Upsilon} w_n \mathbf{F}_n(\boldsymbol{\xi})\right)^{-1}\right) \\ \text{subject to} \quad & \mathbf{1}^T\mathbf{w} \leq N, \\ & w_n \in [0,1], n = 1,2,\dots,\Upsilon = |\mathcal{M}|\end{aligned} \tag{25}$$

where the constraints on $\mathbf{w}$ have been relaxed by allowing it to take on values in the continuous interval $[0,1]$. The resulting relaxed solution will yield a sensor placement, formed by rounding the determined values w_n to either 0 or 1, producing an estimate close to the optimal (combinatorial) solution. As shown in [19], the resulting optimization problem may be reformulated as

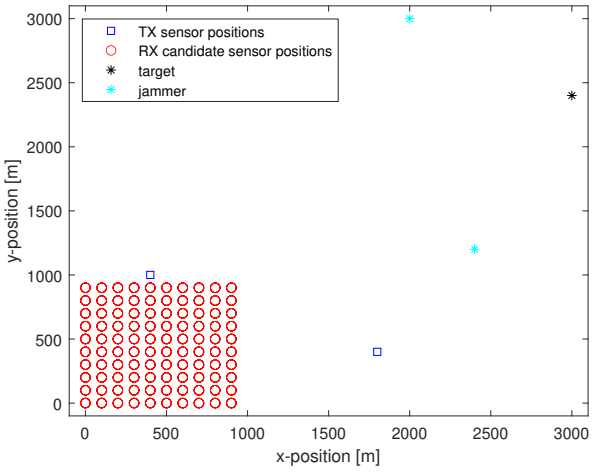

Fig. 1. An illustration of the considered setup, showing the TX locations, the potential RX locations as well as a single target and two jammers.

$$\begin{aligned}\min_{\boldsymbol{\mu},\mathbf{w}} \quad & \sum_{\ell}\psi_\ell\mu_\ell \\ \text{subject to} \quad & \begin{bmatrix}\sum_{n=1}^{\Upsilon} w_n\mathbf{F}_n(\boldsymbol{\xi}) & \mathbf{e}_\ell \\ \mathbf{e}_\ell^T & \mu_\ell\end{bmatrix} \succeq \mathbf{0}, \\ & \sum_{n=1}^{\Upsilon} w_n\mathbf{F}_n(\boldsymbol{\xi}) \succeq \mathbf{0}, \\ & \mathbf{1}^T\mathbf{w} \leq N, w_n \in [0,1],\end{aligned} \tag{26}$$

for $\forall \ell \in \{1, \dots, \mathcal{L}\}$, where ψ_ℓ denotes a weighting factor that may be included to indicate the importance of specific parameters, $\mathcal{L}$ the number of elements in the parameter vector $\boldsymbol{\xi}$, $\mathbf{e}_\ell$ the ℓth canonical basis vector, i.e., a vector containing a 1 at the ℓth position and zeros elsewhere, and with $\mathbf{X} \succeq 0$ denoting that the matrix is positive semidefinite. This constitutes a semidefinite program that may be solved efficiently using standard convex solvers, such as SeDuMi or SDPT3 (see also [20]).

Given that the here considered problem focuses on the identification of the nature of the reflecting target, the parameter of interest here is only the deception ranges, implying that $\psi_\ell = 1$ for $\ell \in \{5, 12, 19\}$, and zero otherwise, for the below examples. The resulting optimization problem will then select the RX sensor candidates that allow for the theoretical minimal variance of the deception range. To allow for an accurate estimate of the deception range, it will necessitate accurate estimates of the other relevant parameters for the reflector. Thus, the selection will clearly not be unsuitable for these other estimates, but by setting the emphasis on only minimizing the theoretical variance of the deception range, the sensor selection will optimize for this parameter.

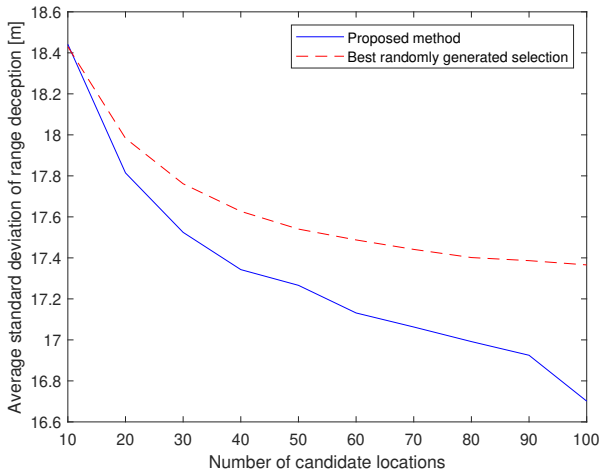

Fig. 2. The minimum achieved standard deviation for the estimate of the deception range using $N = 10$ RX sensors for varying number of candidate locations, using the proposed method, as compared to the best of 10.000 uniformly drawn sensor selections. The result show the average standard deviation for 100 MC simulations over the different candidate locations for an SNR of -10 dB.

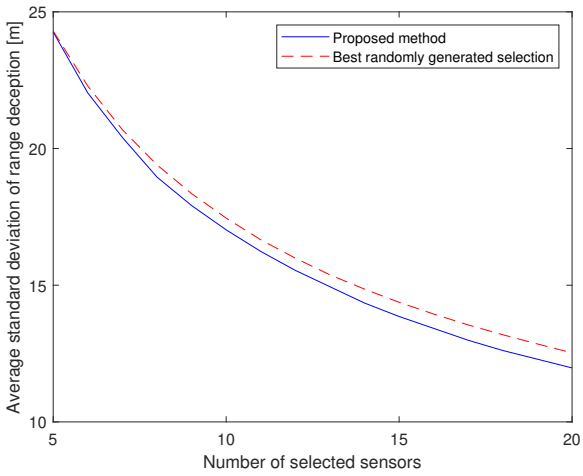

Fig. 3. The minimum achieved standard deviation for the estimate of the deception range, using 60 candidate locations, for varying number of selected RX sensors, using the proposed method, as compared to the best of 10.000 uniformly drawn sensor selections. The result show the average standard deviation for 100 MC simulations over the different candidate locations for an SNR of -10 dB.

IV. Numerical simulations

We proceed to examine the performance of the proposed sensor selection scheme, considering a setup with $M = 2$ TX-antennas, each emitting a chirp-modulated pulse with carrier frequency

$$f_c^m = f_0 + m\Delta f, \tag{27}$$

where $f_0 = 1$ GHz and $\Delta f = 1$ MHz. The emitted pulse length is $T_p = 4$ μs, the sampling frequency $f_s = 15$ MHz, and the bandwidth is $B_s = 1$ MHz. The candidate grid for the RX sensors is a 10-by-10 grid, with each grid point location placed 100 m apart, as illustrated in Figure 1, with each location containing 9 potential candidate positions arranged in a 3-by-3 grid, with an intersensor distance of 0.15 m. In this example, the target state vector is

$$\boldsymbol{\Theta}^1 = \begin{bmatrix} 3000 & 2400 & 40 & 25 & 0 & 0 & 1 \end{bmatrix}^T$$

(with units [m, m, m/s, m/s, m, Hz, 1]), whereas the two jammer state vectors are

$$\boldsymbol{\Theta}^2 = \begin{bmatrix} 2400 & 1200 & 20 & -10 & 100 & 10 & 1 \end{bmatrix}^T,$$
$$\boldsymbol{\Theta}^3 = \begin{bmatrix} 2000 & 3000 & -50 & 30 & 150 & -15 & 1 \end{bmatrix}^T.$$

For simplicity, only a single pulse, $K = 1$, is considered.

Figure 2 illustrates how the standard deviation of the deception range depends on the number of considered candidate locations when selecting $N = 10$ RX sensors, comparing the standar deviation resulting from the proposed method with that of the best of 10.000 uniformly drawn placements. Here, the considered candidates have been drawn (uniformly) from the full 10-by-10 grid (containing 100 locations, each containing 9 potential sensor placements). To avoid bias due to the selection of candidate locations, the shown result for each number of candidates is the average result computed over 100 Monte-Carlo (MC) simulations. As is clear from the figure, the proposed method clearly outperforms the best of the randomly drawn placements, with the gain naturally increasing as the number of considered locations increase.

Figure 3 illustrates the result if one instead varies the number of selected RX sensors for a fixed number of considered locations, here selected to be 60 candidate locations, i.e., for 60 x 9 = 540 potential sensor placements. The result again shows the average standard deviation from 100 MC simulations. As can be seen in the figure, the proposed method is showing a consistent gain as compared to the best random sensor placement, for all number of selected sensors. In these examples, the signal-to-noise ratio (SNR), defined as

$$SNR = 10\log\left(\frac{\text{mean}(|\breve{z}_{mnk}^{qp}|^2)}{\sigma_w^2}\right) \tag{28}$$

has been set to $SNR = -10$ dB, where the mean has been taken over all non-zero samples of the pulse.

As the proposed optimization emphasizes the deception range, not the target localization parameters, the positioning performance of the proposed scheme will be somewhat worse than optimal for localization. As compared to the best localization estimate from 10.000 random sensor selections, this loss is on average 0.02% of the overall position error for the target, for SNR = -10 dB, $N = 10$, and 60 candidate locations, indicating the marginal influence on the positioning by the focused optimization. Finally, Figure 4 illustrates how the performance is affected for varying SNR, for $N = 10$ RX sensors and 60 candidate locations. As expected, the minimal standard deviation can be seen to increase linearly with increasing SNR.

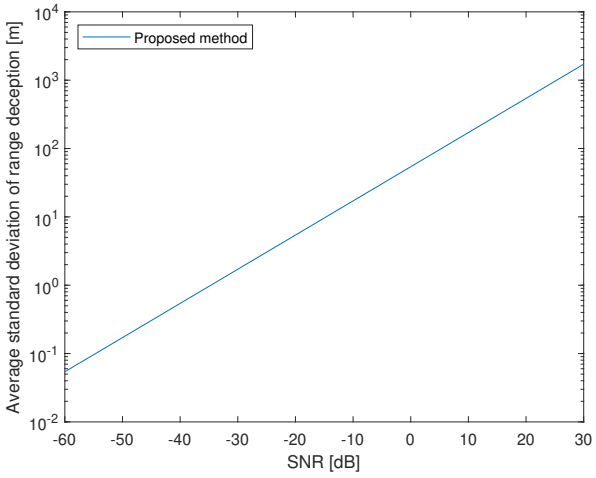

Fig. 4. The minimum achieved standard deviation for the estimate of the deception range using $N = 10$ RX sensors and 60 candidate locations, i.e., 540 potential sensor placements, for varying values of the SNR, using the proposed method. The result show the average standard deviation for 100 MC simulation over the different candidate locations

V. Conclusions

In this paper, we develop an optimal sensor placement scheme for parameter estimation in the presence of deception jamming, which allows individual weighting of the importance of each parameter. This allows us to optimize the sensor placement specifically for the estimation of the deception range, to be used for jammer identification. We compare the proposed method to a randomized method that picks the best sensor placement out of 10.000 different ones, and we show that the proposed method outperforms the randomized method. Lastly, it can be noted that the proposed method will be more useful when there are many candidates to pick from and when many sensors are to be selected.

VI. Acknowledgements

The authors appreciate the helpful discussions with Dr. Jie Cheng. This work was supported in part by the Wallenberg AI, Autonomous Systems and Software Program (WASP) funded by the Knut and Alice Wallenberg Foundations.

References

[1] M .I. Skolnik, *Radar Handbook*, The McGraw-Hill Companies, 2008.

[2] Richard A Poisel, *Information warfare and electronic warfare systems*, Artech House, 2013.

[3] M. Zhang, J. Lu, J. Xu, and S. Li, "Mainlobe deceptive interference suppression with planar frequency diverse array MIMO radar," *IEEE Transactions on Aerospace and Electronic Systems*, pp. 1–13, 2025.

[4] H. Zhang, W. Liu, Q. Zhang, and J. Xie, "Joint resource optimization for a distributed MIMO radar when tracking multiple targets in the presence of deception jamming.," *Elsevier Signal Processing*, vol. 200, 2022.

[5] W.-Q. Wang, H. C. So, and A. Farina, "FDA-MIMO signal processing for mainlobe jammer suppression," in *27th European Signal Processing Conference*, 2019, pp. 1–5.

[6] J. Zhu, S. Zhu, J. Xu, and L. Lan, "Discrimination of target and mainlobe jammers with FDA-MIMO radar," *IEEE Signal Processing Letters*, vol. 30, pp. 583–587, 2023.

[7] Z. Wu, S. Zhu, J. Xu, L. Lan, and M. Zhang, "Interference suppression method with MR-FDA-MIMO radar," *IEEE Transactions on Aerospace and Electronic Systems*, vol. PP, pp. 1–15, 10 2023.

[8] J. Zhang, D. Zhu, and G. Zhang, "New antivelocity deception jamming technique using pulses with adaptive initial phases," *IEEE Transactions on Aerospace and Electronic Systems*, vol. 49, no. 2, pp. 1290–1300, 2013.

[9] C. Wen, J. Peng, Y. Zhou, and J. Wu, "Enhanced three-dimensional joint domain localized STAP for airborne FDA-MIMO radar under dense false-target jamming scenario," *IEEE Sensors Journal*, vol. 18, no. 10, pp. 4154–4166, 2018.

[10] A. Nysaeter, "Adaptive suppression of smart jamming with FDA permutation," in *IEEE Radar Conference*, 2022, pp. 1–5.

[11] L. Lan, G. Liao, J. Xu, Y. Zhang, and F. Fioranelli, "Suppression approach to main-beam deceptive jamming in FDA-MIMO radar using nonhomogeneous sample detection," *IEEE Access*, vol. 6, pp. 34582–34597, 2018.

[12] R. Gui, W.-Q. Wang, A. Farina, and H. C. So, "FDA radar with Doppler-spreading consideration: Mainlobe clutter suppression for blind-Doppler target detection.," *Elsevier Signal Processing*, vol. 179, 2021.

[13] W. Jia, A. Jakobsson, and W.-Q. Wang, "Coherent FDA receiver and joint range–space–time processing," *IEEE Transactions on Antennas and Propagation*, vol. 72, no. 1, pp. 745–755, 2024.

[14] S. Joshi and S. Boyd, "Sensor selection via convex optimization," *IEEE Transactions on Signal Processing*, vol. 57, no. 2, pp. 451–462, 2009.

[15] G. Fatima, P. Stoica, A. Aubry, A. De Maio, and P. Babu, "Optimal placement of the receivers for multistatic target localization," *IEEE Transactions on Radar Systems*, vol. 2, pp. 391–403, 2024.

[16] M. Juhlin and A. Jakobsson, "Optimal sensor placement for localizing structured signal sources.," *Elsevier Signal Processing*, vol. 202, pp. 108679, Jan. 2023.

[17] M. Chen, M. Zhao, A. Liu, M. Li, and Q. Shi, "Joint node selection and resource allocation optimization for cooperative sensing with a shared wireless backhaul.," *IEEE Transactions on Signal Processing*, vol. 73, pp. 67 – 82, 2025.

[18] H. Jiao, J. Yan, W. Pu, Y. Chen, H. Liu, and M.S. Greco, "Wideband sensor resource allocation for extended target tracking and classification.," *IEEE Transactions on Signal Processing*, vol. 73, pp. 55 – 66, 2025.

[19] J. Swärd, F. Elvander, and A. Jakobsson, "Designing sampling schemes for multi-dimensional data," *Elsevier Signal Processing*, vol. 150, pp. 1–10, 9 2018.

[20] F. Elvander, J. Swärd, and A. Jakobsson, "An efficient solver for designing optimal sampling schemes," *ArXiv:2111.05579*, 2021.